Review article **Open Access**

Fulya Ekiz-Kanik*, Derin Deniz Sevenler, Neşe Lortlar Ünlü, Marcella Chiari and M. Selim Ünlü*

Surface chemistry and morphology in single particle optical imaging

DOI 10.1515/nanoph-2016-0184
Received November 23, 2016; revised February 10, 2017; accepted March 20, 2017

Abstract: Biological nanoparticles such as viruses and exosomes are important biomarkers for a range of medical conditions, from infectious diseases to cancer. Biological sensors that detect whole viruses and exosomes with high specificity, yet without additional labeling, are promising because they reduce the complexity of sample preparation and may improve measurement quality by retaining information about nanoscale physical structure of the bio-nanoparticle (BNP). Towards this end, a variety of BNP biosensor technologies have been developed, several of which are capable of enumerating the precise number of detected viruses or exosomes and analyzing physical properties of each individual particle. Optical imaging techniques are promising candidates among broad range of label-free nanoparticle detectors. These imaging BNP sensors detect the binding of single nanoparticles on a flat surface functionalized with a specific capture molecule or an array of multiplexed capture probes. The functionalization step confers all molecular specificity for the sensor's target but can introduce an unforeseen problem; a rough and inhomogeneous surface coating can be a source of noise, as these sensors detect small local changes in optical refractive index. In this paper, we review several optical technologies for label-free BNP detectors with a focus on imaging systems. We compare the surface-imaging methods including dark-field, surface plasmon resonance imaging and interference reflectance imaging. We discuss the importance of ensuring consistently uniform and smooth surface coatings of capture molecules for these types of biosensors and finally summarize several methods that have been developed towards addressing this challenge.

Keywords: optical biosensors; surface morphology; surface modification; single-particle detection; nanoparticle imaging.

1 Introduction

Humans have always been intrigued by the microscopic world. Nearly 400 years ago, Robert Hooke's book of the microscopic world fascinated scientists by providing a glimpse into the previously invisible details of insects and minerals [1]. Advent of optical microscopy has provided detailed visualization and study of biological specimens including cells and bacteria. With the invention of photography, it was possible to capture images of the microscopic biological particles without human intermediaries for recording the visualization under the microscope, and thus, the true meaning of "seeing is believing" has been realized [2]. Today, non-optical microscopes allow us to probe into the once invisible world, and it has become possible to visualize the nanoscale biological particles. A lens-based optical imaging system (conventional light scattering microscopy) cannot discern details that are closer than half of the wavelength of light. However, in fluorescence microscopy – most popular imaging modality for biological specimens – this diffraction limit can be surpassed [3]. That the 2014 Nobel Prize in Chemistry was awarded jointly to Eric Betzig, Stefan W. Hell and William E. Moerner "for the development of super-resolved fluorescence microscopy" is a testimony to the importance of nanoscale observations in the biological world.

Synthetic and natural nanoparticles (NP) – generally defined as having a size of 10–100 nm – have enormous utility as well as potential adverse impact in biotechnology, human health, medicine, and food safety [4–7]. Detection and characterization of biological nanoparticles

***Corresponding authors: Fulya Ekiz-Kanik,** Boston University, Electrical and Computer Engineering Department, Boston, MA 02215, USA, e-mail: fulyaek@bu.edu; and **M. Selim Ünlü,** Boston University, Electrical and Computer Engineering Department, Boston, MA 02215, USA; and Boston University, Biomedical Engineering Department, Boston, MA 02215, USA, e-mail: selim@bu.edu
Derin Deniz Sevenler: Boston University, Biomedical Engineering Department, Boston, MA 02215, USA
Neşe Lortlar Ünlü: Boston University, Biomedical Engineering Department, Boston, MA 02215, USA; and Bahçeşehir University, Faculty of Medicine, Istanbul 34353, Turkey
Marcella Chiari: Consiglio Nazionale delle Ricerche, Istituto di Chimica del Riconoscimento Molecolare (ICRM), Milano, Italy

represent unique challenges and opportunities. Viruses are the most abundant species on earth, with an estimated ~10^{32} phages in the biosphere [8] and ~10^{7} viruses on average in a milliliter of seawater [9]. The detection and identification of individual virions are of significant interest due to their potential relation with many infectious diseases and human cancers [10]. Early and sensitive detection of infections is important especially for high impact diseases leading to epidemics. Consequently, many detection systems for viral diagnostics have been developed during the outbreaks [11]. Along with the infectious diseases, viruses are considered to be linked with many human cancers. Although the specific mechanisms leading to cancer subsequent to infection with the particular viruses are not always clear and established, usually, a single virion is found to be the responsible [10]. In addition, it is important to detect the biological nanoparticles in their innate environment such as in serum or other bodily fluids without altering the physiological conditions in order to be more accurate and free of manipulation during the detection. Consequently, there is always a need for single-particle detection systems that are robust, affordable, high-throughput, sensitive in heterogeneous media, and less technically difficult.

The structure and size of viruses vary in a wide range with high complexity in shape. They are found in various forms such as long or short rods, spheres, spheroids, or spheroids with tails. Not many of viruses are in uniform size [12]. Also, for particular viruses, variation in particle size is a phenotypical characteristic. Hence, structural information is significant in classifying viruses. Understanding structure and size gives further information about the mechanisms of certain biological processes and interaction of the virus particles with the cell receptors and antibodies in the blood stream. The size of viruses varies from 20 nm to 300 nm [13]. In particular, the smallest viruses so far are found to be around 18–22 nm in diameter [14], only slightly smaller than the human antibodies with an average size of 12 nm [15, 16]. While the commonly used detection methods for virus detection are conventional immunoassays and polymerase chain reaction (PCR), the former assay is limited with quantification problems and the latter requires well-established tools with high instrumentation costs and experienced labor. Neither of the conventional diagnosis assays provide any information about the size or shape of the virus.

Another class of abundant biological nanoparticles is exosomes, which are phospholipid nanovesicles that are secreted by mammalian cells [17]. The interest towards these vesicles of has grown exponentially over the last several years following the discovery that they are involved in intercellular communication by serving as transfer vehicles of proteins, mRNA, and miRNA between cells [18]. Their size changes in a range of 30 nm–100 nm [19, 20]. Recent studies have shown that a large number of exosomes are released from the cells in most types of cancer, which reserve molecular information about the original tumor [21]. Detection and identification of exosomes are challenging due to cumbersome purification steps and the requirement for labeling. Conventional isolation and detection techniques such as enzyme-linked immunosorbent assays (ELISA) and Western blot are usually time consuming and require large sample volumes, isolation, and post-isolation steps.

In summary, both viruses and exosomes are of vital interest for biological studies, and they represent similar challenges in detection and visualization due to their small size and low refractive index contrast. Due to the growing need in rapid detection and quantification, there has been a significant interest in the development of sensors for biological nanoparticles. For reliable results, it is crucial to detect them with high sensitivity. Fluorescence-based microscopy techniques have been developed extensively for detection of biological nanoparticles and molecules [22, 23]. They require fluorescence labeling of the single natural nanoparticles, which makes them less applicable for a variety of samples. Moreover, nonspecific binding of the fluorescent labels to the other components in the heterogeneous media or formation of aggregates remains as a challenge in fluorescence detection systems along with the inconstancy of the fluorescence signal independent of the size of the biological nanoparticles [24]. Also, irreversible photobleaching of the fluorescent label limits observation time. Electrical sensors also provide single virus or biological particle detection. However, as they are very dependent to the environmental conditions and the properties and content of the sample media such as pH, heterogeneity, and changes in ionic strength, they suffer from specificity and selectivity issues [25, 26].

Optical biosensors are highlighted with their distinct properties and advantages such as high sensitivity, easy adaptation to multiplexed systems, and portable operation capability [27, 28]. They are also attractive due to their non-invasive nature. Elastic light scattering-based direct detection methods that require no molecular labels are more advantageous than fluorescence methods that may suffer from variability and temporal decay of the signal due to photobleaching. However, as the elastically scattered light intensity induced by the illumination of the nanoparticles scales with the sixth power of the particle size, it is very difficult to detect small biological nanoparticles over the background scattering [29, 30]. Consequently,

eliminating the background noise for small particle detection is of vital importance.

In this review, we discuss emerging optical biosensor techniques for detection of biological nanoparticles with particular attention to label-free methods in imaging modality. Our focus is on bio-nanoparticles (BNPs) that are smaller than 100 nm in size and have low refractive index contrast with respect to the surrounding medium. Many of the emerging optical techniques rely on capturing BNPs on sensor surfaces and image enhancement by a variety of methods including background reduction as in dark-field microscopy, imaging surface plasmon resonance, and interferometry. The study of BNPs has two modalities: detection and characterization. For detection, it is critical to have visibility of the nanoparticles with sufficient signal-to-noise ratio. Discrimination from the background is necessary for accurate detection to avoid false positives. For light-scattering-based direct detection, discrimination often requires coarse size determination. In case of characterization, light-scattering techniques must provide more detailed information about the physical properties including size and shape of BNPs. The inability of light-microscopy in providing chemical specificity is overcome by using sensor surfaces with specific capture probe molecules such as antibodies or aptamers. Within the context of this multi-faceted challenge, we explore the influence of a common denominator – surface morphology. Clearly, to detect the presence of a 30–100-nm biological nanoparticle on a sensor surface and characterize its physical properties (size and shape), the morphology of the surface must be carefully considered. We address limitations due to surface roughness, consider the implications for different optical imaging techniques, and discuss various surface preparation methods to overcome the challenges imparted by the roughness of conventional antibody surfaces.

2 Label-free optical imaging detectors of single biological nanoparticles

Conventional light scattering microscopy cannot resolve features much smaller than the illumination wavelength due to the diffraction limit. When we consider imaging a sensor surface with a sparse distribution of nanoparticles, classical understanding of optical resolution may no longer be the primary concern. In this case, objects of interest, i.e. nanoparticles, may not be visible above the background, as they scatter light very weakly. Radioisotope and fluorescence staining, therefore, have historically been used to "decorate" or "label" biological nanoparticles and increase their visibility. These labels can add molecular specificity (for example, by using a fluorescently labeled antibody or complementary oligonucleotide), but they may hinder characterization of physical properties and also increase assay complexity and cost. To address applications where these are major concerns, a variety of label-free assays for BNPs have been developed. Many of these techniques utilize light and, either directly or indirectly, detect light scattered by the BNP. Label-free optical imaging biosensors are those that use imaging optics to rapidly measure a large sensor surface area. In this section, we describe three members of the family of label-free optical imaging biosensors, which are dark-field microscopy (DF/TIRM), surface plasmon resonance imaging (SPRi), and interference reflectance imaging (IRIS, iSCAT) [31–34]. We also introduce the notion that for label-free imaging approaches, even more than for other types of label-free sensors, the surface morphology of the sensor's functionalization is extremely important. Table 1 shows a comparison of label-free optical imaging biosensors utilized in the detection of BNP. The implementation and availability of these technologies at diagnosis near-patient are also shown. Point-of-care (POC) testing requires miniaturized, portable platforms and avoidance of time-consuming steps of analysis. Among these technologies, dark-field microscopy and iSCAT are not deployable to majority of clinical locations at POC. While SPRi is very sensitive and highly employed, the use of SPRi has not yet been demonstrated at POC. On the other hand, SP-IRIS has POC capability for virus detection. It allows virus detection in complex media via the use of disposable cartridges and a benchtop-size microscope with minimal sample and reduced exposure risk [40].

2.1 Label-free optical imaging biosensors are capable of specific detection of individual biological nanoparticles

A variety of more advanced and sensitive optical systems have been developed towards the goal of developing label-free detection of BNPs. This genus of optical biosensors can be further divided into surface-imaging and non-imaging methods. Surface-imaging sensors usually involve some type of far-field microscope, which detects the binding of individual nanoparticles to a relatively large (100–1,000,000 square microns) sensor surface. We consider non-imaging optical methods to include all optically

Table 1: A comparison of label-free optical imaging biosensors in detection of biological nanoparticles.

Technology	Optical system	Analyte	Matrix	Detection limit	Availability at point of care	Advantages	Ref.
Dark-field microscopy	Total internal reflection dark-field microscopy	Influenza virus	Buffer	1.26×10^{4} pfu/ml	Not applicable	Simple optical system and no elaborated sample preparation required	[31]
Surface plasmon resonance	Surface plasmon resonance imaging	HIV-based virus-like particles	Buffer	–	Applicable but not shown yet	Efficient for quantification and characterization of BNPs	[35]
	Surface plasmon resonance imaging	Influenza A virus	Buffer	0.2 fg/mm^2	Applicable but not shown yet	Mass/size measurement of single viral particles	[36]
Interference reflectance imaging	iSCAT	Lipid nanodomains responsible in cell signaling	Lipid-oil solution	Tracking individual domains in lifetime of 0.22 ± 0.06 s	Not applicable	Time-lapse imaging of dynamic creation and destruction of lipid nanodomains	[37]
	SP-IRIS	Exosomes from a HEK293 cells	Buffer	3.94×10^{9} particles/ml	Not applicable	Phenotyping and characterization of exosomes directly from human cerebrospinal fluid	[38]
	SP-IRIS	Recombinant vesicular stomatitis virus Ebola model	100% Fetal bovine serum	100 pfu/ml	Applicable	Real-time imaging of individual viruses, highly sensitive rapid detection platform of pathogens with minimal sample preparation	[39]
	SP-IRIS	Ebola virus, Zaire strain-variant Mayinga	100% Fetal bovine serum	1×10^{5} pfu/ml	Very applicable	Disposable polymer-paper fluidic cartridge capable of sensitive and specific viruses, detection limit 10–100 times more sensitive than commercial rapid tests	[40]

resonant micro- or nano-structures that utilize diffraction gratings, micro-ring, micro-toroid, liquid-core, and whispering-gallery-mode resonators and other optical resonator devices. Many of these non-imaging approaches have been used to transduce the binding of single BNPs [41, 42]. However, they are qualitatively different from surface-imaging methods; they generally have a functionalized capture surface that is orders of magnitude smaller than surface-imaging sensors and are usually capable sampling at much higher frequency. As such, the challenges in surface functionalization and signal-to-noise associated with those sensors are entirely different from those of imaging sensors. As an example, non-imaging resonant sensors tend to excel in studies of single-nanoparticle and even single-molecule interactions at the millisecond scale in a controlled solution [43]. However, surface-imaging sensors tend to be better suited for highly sensitive and multiplexed tests requiring large dynamic range in chemically complex or unknown sample solution, which are often characteristic requirements of diagnostic tests [38]. Our discussion herein is limited to surface-imaging biosensors and the impact of the morphology of surface coatings (functionalization) on their performance.

Label-free imaging BNP detectors generally employ at least one of the following optical enhancement techniques to improve the signal-to-noise ratio: (a) background light rejection, (b) surface plasmon resonance, or (c) interferometric detection. In the following three sections, we describe and compare each of these techniques in detail.

2.2 Application of dark-field microscopy to BNP detection

In dark-field illumination methods, the illumination and imaging optics are configured in a way to reject specular reflection from planar surfaces and collect only scattered light from objects of interest. In this configuration, weak scattering objects such as BNPs can be visualized. An effective method of providing dark-field illumination is to utilize total internal reflection, in which case, scattering from BNP converts the otherwise non-propagating (evanescent) excitation to propagating fields that can be collected and imaged in the optical far field.

Label-free optical imaging and quantitative detection of virus particles *via* total internal reflection dark-field microscopy have been demonstrated [31]. Real-time imaging can be performed by illuminating the virus particles on the surface with an evanescent field and collecting the scattered light from the individual particles as seen in Figure 1. The intensity of the scattered light reflects the

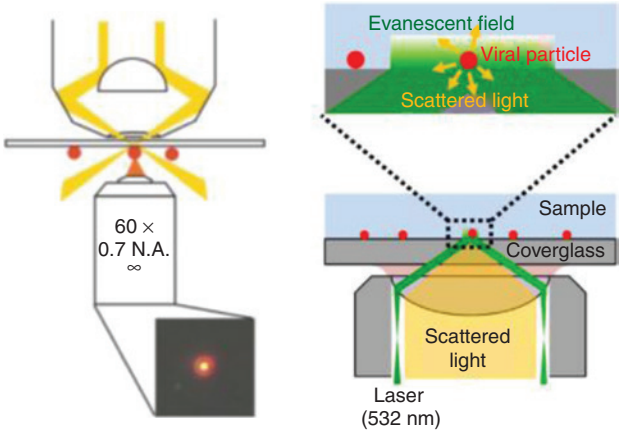

Figure 1: A schematic of two dark-field microscopy configurations. Left: A dark-field condenser illuminates the substrate at angles higher than the collection numerical aperture. Only scattered light is collected, resulting in images with a dark background. Right: Excitation light from a dark-field immersion epi-objective is totally internally reflected at the coverglass-sample interface. While a dark-field condenser allows detection of nanoparticles anywhere within a thick transparent sample, TIRM tends to have better stray light rejection but is limited to detecting particles within about 200 nm of the coverglass-sample interface. (Left: Adapted from [44]. Right: Adapted from [31]).

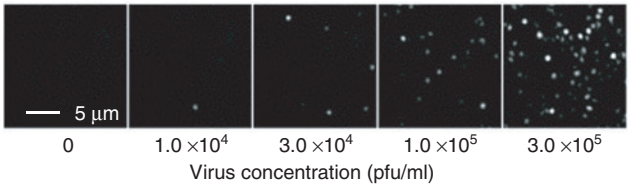

Figure 2: Example images from a total internal reflection microscope (TIRM) as individual human immunodeficiency virus particles are captured onto a functionalized coverglass surface. Adapted from [31].

virus concentration in the sample. As seen in Figure 2, virus particles appear on the glass surfaces as diffraction-limited spots [31].

2.3 Application of surface plasmon resonance imaging to BNP detection

An elegant method of providing dark-field illumination and enhanced optical response to biological binding of nanoparticles on the sensor surface is achieved by surface plasmon resonance imaging (SPRi). In SPR, illumination is incident from a high refractive index medium at an angle larger than that of the total internal reflection as shown in Figure 3. In the immediate vicinity of the interface, there is a decaying (evanescent wave) field in the low index material (typically the target solution) [45]. At the interface of a metal and a dielectric, oscillation of the free accumulated electrons creates surface plasmons (SPs). At a particular incidence angle, p-polarized incident wave is resonantly coupled into SPs causing a remarkable dip in the reflectivity signal [46]. The resonance condition is highly sensitive to local dielectric behavior within the extent of the evanescent field penetrating into the target solution. Thus, the binding of single BNPs can be detected in a label-free manner. Although SPR is a very sensitive method, it necessitates strict requirements for material properties and optical configuration. Among the available metals for SPR applications, generally, gold is used due to its stability and durability in various applications [47]. SPR principle is applied in many fields including high-throughput screening, especially in detection of proteins, biological nanoparticles, and DNA sequences based on protein-protein interactions, antibody-antigen interactions, cell receptor-ligand interactions, and compliance of DNA sequences. In imaging modality (SPRi), the sensor surface is visualized *via* a CCD camera. After the modification of the sensor surface with the surface probes, images of the sensor surface are taken, which reveal the local changes on the surface (Figure 4).

2.4 Application of interference reflectance imaging to BNP detection

Interference reflectance imaging is a technique in optical microscopy for improving the visibility of small inhomogeneities in or on layered substrates, for example, in cell microscopy [49] and integrated circuit inspection [50, 51]. Interference reflectance imaging has been utilized in several label-free biosensor designs, namely, by the Gauglitz group as Reflectance Interference Spectroscopy (RIfS), Sandoghdar group as Interferometric Scattering Microscopy (iSCAT), and Ünlü group as the Interference Reflectance Imaging Sensor (IRIS) [34, 52, 53]. All of these techniques measure the binding of biomolecules as small changes in the reflectivity or reflectivity spectrum of a layered substrate. The specific accumulation of biomolecules to the topmost layer in the substrate changes the local refractive index, effectively acting as an additional layer and thereby changing the reflectance spectrum of the entire substrate in a predictable manner. These three techniques use slightly different optical configurations, each yielding advantages and disadvantages. In previous-generation designs, both RIfS and IRIS measured the reflectance spectrum of a thin film substrate by using either a white light illumination and an imaging

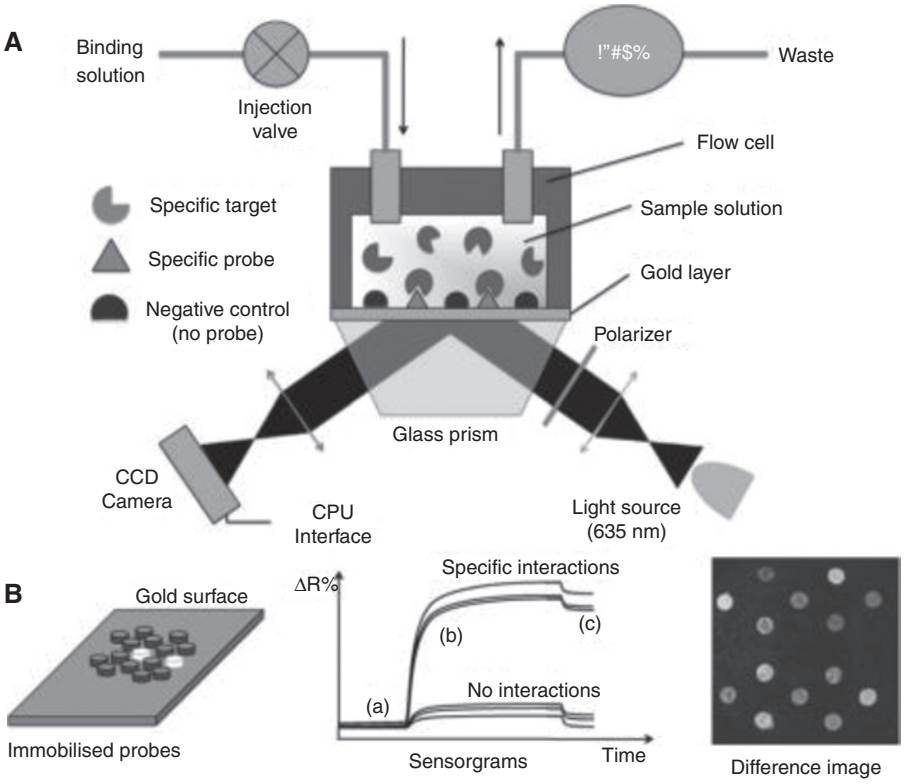

Figure 3: A typical SPRi instrument configuration. A gold film is coated onto one face of a glass prism, then prepared with a microarray of different capture "probes", and finally exposed to the sample solution. The binding of analytes to the surface changes the local refractive index (RI), which is detected *via* a corresponding change in the backside reflectivity of the film by a p-polarized laser beam. The illuminating beam is configured to excite surface plasmon polaritons in the gold film, which are highly sensitive to changes in local RI. Adapted from [32].

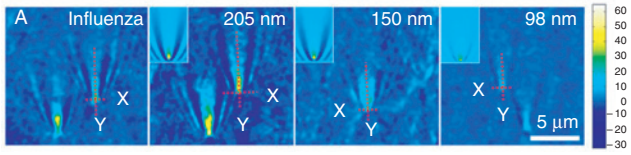

Figure 4: Individual influenza virus particles and differently sized silica nanoparticles are immobilized onto a chromium and gold-coated coverslip and detected with surface-plasmon resonance microscopy. SPR waves induced by TIR illumination are diffracted by any inhomogeneities in the gold. Adapted from [48].

spectrometer (RIfS) or sequential illumination with different wavelengths of light (IRIS) [52, 54]. Both technologies have since switched to single-wavelength illumination from a light-emitting diode, as this approach allows the highest signal-to-noise and greatly improves processing speed when measuring small amounts of analyte [36, 55].

The challenge of detecting light scattered by individual BNPs is conceptually different from that of label-free biosensors described earlier. As BNPs are usually less than 200 nm in diameter, their scattered light intensity is very often less than 0.01% the intensity of the incident illumination [33]. Mixing the scattered light field with a reference light beam, just as in a homodyne or heterodyne interferometer, allows such a particle to be detected as a faint, a weak but discernible change (in the order of 1%) in the intensity of the reference field. Provided that the reference field is sufficiently uniform and consistent and shot noise is sufficiently low, image processing software can automatically and consistently detect 1% contrast features in otherwise featureless surface region.

Both IRIS and iSCAT have been used to detect single BNPs, although with very different applications, resolution, and time scales [39, 56]. The single particle IRIS (SP-IRIS) instrument is virtually identical to IRIS, except that it utilizes a higher NA objective (typically 0.8–0.9). As SP-IRIS uses an LED with a temporal coherence length of only about 10–30 microns, it is possible to achieve a highly uniform illumination field *via* Köhler illumination. Both IRIS and SP-IRIS utilize polished silicon substrates, upon which 100 nm of thermally grown silicon dioxide. Polished silicon wafer production and thermal oxide growth are standard processes in semiconductor manufacturing, so IRIS substrates are quite affordable, costing about \$0.30–\$3.00 for a 12×25-mm chip. Single biological nanoparticles result in small, diffraction-limited

perturbations in the reflected field, between 0.5% (around 60-nm diameter) and 10% (around 150-nm diameter). The excellent flatness and smoothness of the Si-SiO_2 substrate is a critical component for SP-IRIS, because it enables the detection of diffraction-limited spots that are only 0.5% dimmer (or brighter, depending on the objective's plane of focus [24]) than the reference field even in the absence of dynamic measurements. This in turn allows the stage to be scanned, which enables a region of interest much larger than a single field of view. Figure 5 shows a schematic of an SP-IRIS microscope with a scanning XYZ stage. This instrument can detect captured BNPs across 30 microarray spots (i.e. a total area of several square millimeters) in 5 min, with the potential to image hundreds of spots. The impact of automated, large-area scanning is twofold. First, this enables multiplexed testing *via* microarray printing. Second, this enables the use of a larger sensor surface area for each target BNP, thereby increasing overall sensitivity.

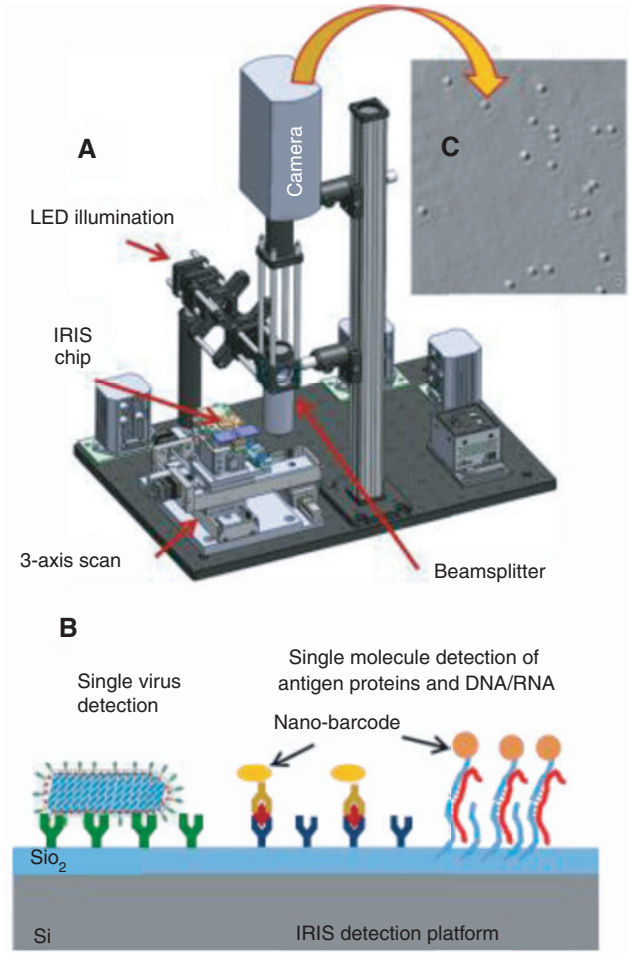

Figure 5: (A) The single particle interference reflectance imaging sensor (SP-IRIS) instrument layout and (B) schematic of substrate and surface coatings. Wide-field epi-illumination is reflected by the thin film substrate, and individual BNPs are detected as diffraction-limited perturbations to the reflected field. Beyond label-free detection of individual BNPs, functionalized metallic nanoparticles may be used as single-molecule labels. Adapted from [24].

Where SP-IRIS uses a partially coherent LED illumination, iSCAT uses a highly coherent laser beam. Wide-field coherent light imaging is nontrivial because of long-range interference effects and laser speckle – to overcome these, a ground-glass diffuser with temporal averaging may be used to ameliorate these effects, provided the exposure time is sufficiently long [34]. A second option is to limit detection to dynamic measurements, in which sequential images are subtracted pixelwise, yielding highly sensitive detection of small changes in what is an otherwise highly nonuniform illumination field [53]. A third, widely used option is to instead focus the illumination to a diffraction-limited spot and scan the focused beam throughout the object plane region of interest [57]. In this third case, a reference photodiode may be used to account for temporal variation in beam intensity, if necessary.

Like iSCAT, SP-IRIS may also be used to perform dynamic measurements of BNP binding in real time. This has enabled rapid tests for hemorrhagic fever viruses such as Ebola shown in Figure 6 [39]. Dynamic measurements with IRIS were a greater challenge as they require front-side imaging as well as high NA. These motivated the design of a custom microfluidic cartridge with a clearance of less than 300 microns between the chip surface and the nose of the microscope objective, which was eventually achieved with a multilayer structure of precut laminates mounted on an acrylic base. Discrimination of individual BNPs in liquid is slightly more challenging than on a dry substrate because the nanoparticle's scattering cross-section is proportional to the difference in refractive indices of the particle and its medium. Roughly speaking, the scattering cross-section of a biological particle ($n \approx 1.4$–1.6) in water ($n \approx 1.33$) is about one-half of the same particle immersed in air ($n \approx 1$). Nevertheless, real-time detection has improved SP-IRIS sensitivity and specificity for single BNPs in two ways. First, the ability to collect more data by imaging the same spot many times during the assay allows a much more accurate measurement of the particle binding rate, which was assumed to be linearly proportional with the target BNP's concentration in solution. Second, it allows for a significant increase in dynamic range. Note that an SP-IRIS measurement is saturated when so many BNPs are captured to the surface that they are too close to distinguish and count individually. Only a real-time assay can distinguish (in a single experiment) between a solution that saturates the sensor in 5 min and one that saturates the sensor in 1 h, for example. The third way in which

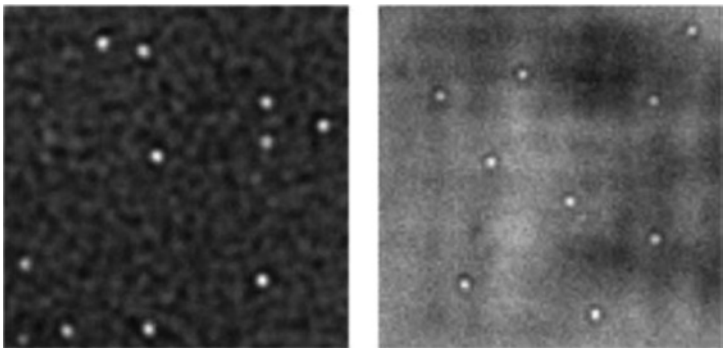

Figure 6: An example readout from an interference reflectance imaging sensor (SP-IRIS) when the substrate is dry (left, 0.8 NA) or when the substrate is mounted in a microfluidic chamber and immersed in water (right, 0.9 NA). Individual vesicular stomatitis virions are detected as small (about 1–3%) diffraction-limited modulations to a reflected reference field. Small fluctuations in the intensity of the reflected reference field are visible in both images. Displayed regions are about 8×8 microns. Adapted from [39] (Reprinted with permission from [39], Copyright 2016 American Chemical Society).

in-liquid dynamic measurement has improved sensitivity is by removing the need to dry the surface before imaging. In our experience, we suspect that surface tension associated with drying may be strong enough to cause some de-binding of weakly-bound BNPs. Altogether, dynamic measurements with SP-IRIS combine high sensitivity and molecular specificity with multiplexed detection, which are crucial for medical diagnostics.

The detection of faint (1–3%), diffraction-limited features in the reflected reference field is made extremely difficult if the reference field is no longer homogeneous and uniform. Unfortunately, surface functionalization can cause highly nonuniform coatings unless certain precautions are taken (Figure 7). For example, protein microarrays prepared by micro-droplet arrayers can have unexpectedly large, non-uniform spots, even after several rounds of optimization. The variable presence of BNP-like features on some spots has posed a significant challenge to developing automatic and robust particle-counting software. The development of surface chemistries, which improves the optical uniformity of spots, as well as improves repeatability for different spotted proteins, has been an unexpectedly important step for the translation of these biosensors to commercial application [58].

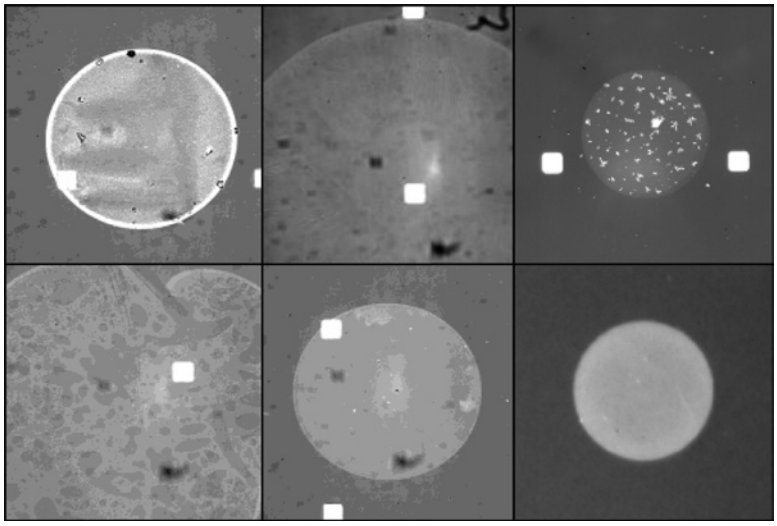

Figure 7: Protein microarray "spots" printed by a microdroplet arrayer can be highly heterogeneous and uneven, which can be a source of noise for label-free detection of BNPs. Depending on the spotting solution contents and the surface material, deposited droplets may dry to form spots with small diffraction-limited islands (top left), striations (top center), multi-scale heterogeneities (bottom left), and isolated regions of high immobilization (bottom center, near the top, and right edges of the spot). They may also accumulate salt deposits (top right). Contrast these poor spots with the one at the bottom right, which is very smooth, uniform, and flat. Developing a virus particle counting software that can filter out all of these types of features has been a significant challenge. Shown regions are 200×200 microns.

3 Surface morphology and immobilization of the surface probes in optical biosensing

In the most general sense, optical biosensors all utilize changes in scattering caused by either local or distributed changes in refractive index. Because the binding of nanoparticles to the sensor surface is detected as small local changes, the temporal and spatial variability of a system's baseline or reference signal limits the smallness of particles it can reliably detect. More generally, this source of noise limits the signal-to-noise ratio for any particle of interest. Hence, reducing this source of noise improves sensitivity in nearly all cases.

Cells and cellular components are optically inhomogeneous, stemming from heterogeneity across multiple length scales. As an example, cytoplasm has a refractive index of 1.38, whereas that of a cell membrane is around 1.48 [59, 60]. Other structures in the cells, such as protein, have variable refractive indices ranging from that of the cell medium and up to as high as 1.53 [61]. The differentiation of target BNPs from such a complex background is a major challenge in label-free detection of BNPs.

3.1 Immobilization of probes and effect of sensor preparation

In solid-state (i.e. solid-phase) biosensor design, a crucial step is the biochemical preparation of the sensor surface to have molecular affinity for the target molecular or BNP. As discussed earlier, both the chemical functionality and surface morphology of the sensor surface impact the performance of label-free optical imaging biosensors. A proper biosensor surface has three key features that facilitate stable and significant responses during long analyses. First, the sensing molecule (also called the "capture probe") must maintain its native reactivity throughout the measurement. Second, the signal coming from the target particle must be larger enough than the background and sensor surface roughness. Third, the modified sensor surface must be selective and specific to the target BNP, interacting strongly with the target BNP yet non-fouling when exposed to a heterogeneous sample. Changes in scattering from nonspecific binding may overwhelm that of target BNPs, reducing sensitivity and resolution. Moreover, nonspecific binding may prevent BNP binding through steric hindrance. Therefore, to obtain a successful and robust assay, a strong immobilization of the sensing element on the assay surface and low background signal are required. Prior to single-particle detection, surface morphology should be measured with high sensitivity to determine the limitations in the measurements.

The key concept in biosensing is to modify the sensor surface with one of the two interacting partners, while the other is ready to be detected in the media. The intensity of the signal is proportional to the amount of captured analyte on the surface, which mostly depends on the probe-target affinity and morphology of the surface. The requirements for a proper sensor surface can be approached by a convenient surface chemistry and immobilization of the biological probes. The surface immobilization has a vital influence on the nature of the interaction. Moreover, external labels may be used for detection of the target particles. This technique enables the selective detection of proteins, nucleic acids, or viruses *via* specific interactions between proteins, complementary nucleic acids, and their receptor proteins, respectively, with high sensitivity, even in real-time measurements [39, 61, 62]. On this basis, controlled immobilization of the surface probes and quality checking of the sensor surface are important for monitoring and characterization of these optical processes.

Determining the best immobilization technique for the application is extremely important. Conventional techniques for biomolecule immobilization include covalent binding and adsorption based on non-covalent interactions such as hydrophobic or electrostatic forces. In the former case, in order to form the covalent linkage, the sensor surface and the biomolecule must bear corresponding functional groups in their chemical structures. The decisive point here is to protect the right orientation and function of the biomolecules after the covalent bonds are formed. In order to have the biomolecule fully functioning on the sensor surface after immobilization, it must preserve its three-dimensional structure and reactivity with the complementary molecule.

Usually, antibodies or nucleic acids are used as surface probes for label-free biosensing. Surface functionalization with proteins is generally more complex and difficult than with nucleic acids due to their structural complexity along with the high number of various functional groups. For receptor proteins, antibodies, and enzymes, retaining the protein's secondary structure as well as binding site availability is necessary for maintaining function [63]. Antibodies are the most commonly used proteins for detection due to their specificities and high binding affinities. They are routinely isolated and manufactured for almost any macromolecules and used against many infectious agents [64]. Other types of proteins and carbohydrate-based probes with, in general, lower selectivity are also used in

virus detection, for example, glycan molecules in influenza detection [65].

Nucleic acid-based probes are used in DNA microarrays for many diseases and virus detection [66]. Orientation and stability are also important in nucleic acid immobilization on the surfaces. The surface of the optical detector is modified with a single-stranded or hairpin-like synthetic oligonucleotide, which has a sequence complementary to a target sequence wanted to be measured in the sample. *Via* hybridization of the DNA surface probe with the target DNA, the change can be detected with a label or label-free in the optical system. As the thermodynamics of hybridization on the solid surface are different than those in solution, surface chemistry is even more crucial in modification of biosensor surface with DNA probes [67]. Adaptation of the conventional techniques of calorimetry and melting curve analysis to surface immobilized probes is difficult for hybridization controls. However, characterization of DNA films on the sensor surface must be determined before the experiments for layer stability, structural arrangement, and quality of the immobilized probes. Immobilized probe layer morphology and stability are important issues especially in sample applications in which many species compete for binding the surface probes along with the target sequence [68].

3.2 Importance of surface morphology in single particle optical imaging

Aside from selecting the proper surface chemistry, biofunctionalization of the sensor surface should be measured systematically. Procedures for biomolecule immobilization are employed in similar ways with the same principles; however, surfaces are usually poorly characterized. Any modification on the sensor may change the ability of the device to detect biomolecules. For instance, in optical resonators, the lowest possibly detectable concentration of the target in sample is usually proportional with the resonance linewidth (also called quality factor) [69]. Poor surface chemistry may cause an increase in linewidth, however, which increases the detection limit [70]. As surface biofunctionalization may occur in multiple steps, it is important to track these changes on the surface in each step and optimize accordingly [71].

In surface plasmon resonance biosensors, microorganisms and viruses can be detected *via* local changes in the refractive index. Due to the confinement of surface plasmon polaritons (SPPs) to within 100–200 nm of the gold-liquid interface, however, only a portion of the entire bacteria is detectable. For the same reason, the sensitivity of these types of biosensors also depends on the separation distance between the target BNP and the gold film. Furthermore, BNPs with a diameter larger than about the evanescent field decay constant are measured with decreasing sensitivity [46]. Hence, surface morphology must be designed accordingly. Despite being one of the most applied optical imaging techniques for BNPs, some limitations constrain SPR-based imaging systems. Having a few hundred-nanometer penetration depth of the evanescent field into the dielectric medium limits the detection of smaller sized particles [72].

SPR imaging (SPRi) enables multiplexed and real-time measurements [32, 73]. However, sensitivity is a limiting issue in SPRi compared to the conventional SPR due to the difficulties in sample delivery in real time over the multiplexed spotted sensor surface. The use of microfluidic flow cells and the amplification of the signal with various techniques improve signal-to-noise ratio in many applications [73–77]. The effective thickness of the captured target layer is the layer of analyte on top of the surface probes on the SPR sensor, which has the major effect on the magnitude of SPR response. The measurements are based on the uniformity and consistency of these two layers on the sensor. However, the refractive index change within the layers also affects the SPR shift in the system. In conventional SPR imaging system designs, it is hard to keep the immobilized probe layer fixed and free of variations, due to the possible non-specific bindings and changes in the surface chemistry of the layer in real-time measurements.

Although the noise is an issue and relatively greater than in SPR, SPRi is utilized in many applications for detection of cells and bacteria [78, 79]. In one approach, the SPRi sensor surface was modified with a hydrogel-based interaction layer. When red blood cell-surface antibody interaction is investigated real time, it was found that the noise level was very high due to the non-specific binding and remaining total mass of cell debris on the surface [79]. As a result, only limited number of cell binding was detected.

Until recently, SPRi was not in use for detection of nanoscale BNPs due to certain limitations. Mainly, restrictions stemming from lateral resolution, SPR-based sensors remained useless for detection of viruses and virus-like particles [78]. However, in 2010, Wang et al. showed that with the right surface chemistry and functionalization, imaging and detection of virus particles on SPRi surface are achievable [48]. The diffraction patterns created by surface plasmon waves of the individual viral particle scattering were used to identify the particles and distinguish them from the background noise and interference patterns. As the intensity of diffraction pattern increases

with the size of the BNP, they were also able to measure the size of the BNP. They have compared influenza A virus (IAV) particles versus artificial silica nanoparticles. Even though synthetic nanoparticles do not adhere to the surface and disappear in real-time imaging measurements, when they functionalized the sensor surface properly, they can capture, image, and count the viral particles on the surface. They obtained a non-specific and irreversible adsorption of the viral particles on the bare gold sensor surface. On the other hand, when they compared different surface modification such as PEGylation and antibody coating, they obtained lower intensity profiles. Even though PEG coating is usually used to prevent non-specific binding and increase the sensitivity by lowering the background, in this particular case, on PEGylated surface, viral particles were observed as transient events, which shows the effect and diversity of surface morphology for each technique and target. Also, anti-influenza A antibody-coated surfaces provided reversible binding in real-time measurements. As seen in Figure 8A, different

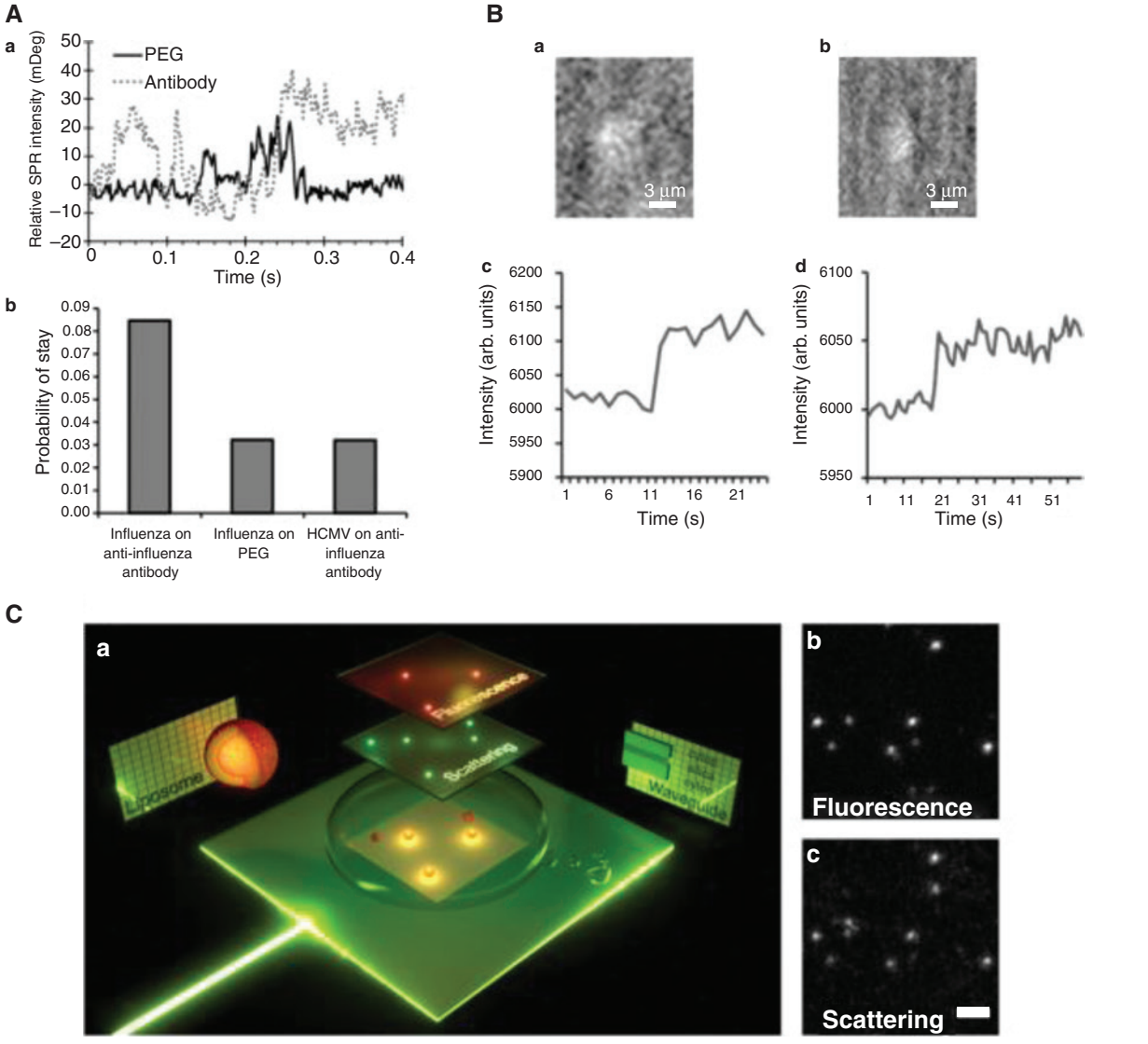

Figure 8: (A) (a) SPR intensity profiles for influenza A viral particles captured on PEG and anti-influenza A antibody-functionalized sensor surfaces. (b) Relative binding probabilities of influenza A on PEG and anti-influenza A antibody-functionalized surfaces, and binding of a different virus HCMV on anti-influenza antibody spots as a control. Adapted from [48]. (B) A SPRi micrograph of (a) IAV or (b) HIV-VLP captured functionalized surfaces. Viruses appear as bright spots on grey background. Intensity change with the binding event of IAV and HIV-VLPs is seen in (c) and (d) as signal increase, respectively. Adapted from [35]. (C) (a) Schematic representation of the planar waveguide chip and detection of fluorescently labeled vesicles in (b) fluorescence and (c) scattering modes. Adapted from [80] (Reprinted with permission from [80], Copyright 2015 American Chemical Society).

surface modifications created different signal intensities. Even though bare gold sensor had more capture, it cannot differentiate between the virus types, whereas anti-influenza A antibody modified surface was applied successfully for influenza A virus capture and remained fairly inert to the other type of virus, HCMV, yielding specific binding and significantly higher signal than the nonspecific bindings. By improving surface properties and system stability, the noise was reduced and they obtained a noise level of 0.3 mDeg, which can detect 13-nm-sized nanoparticles. The imaging intensities of the viral particles were used to determine their size, which was found as 109 ± 13 nm.

In another study, viral particles were counted using SPRi [35]. When the viral particles were captured on the sensor surface, they appeared as bright dots on the background and counted in a very small field of view to improve the detection limit and block the signals coming from the other regions. The authors have showed that they can detect various concentrations of human immunodeficiency virus-like particles (HIV-VLP – spherical, 100–140 nm in diameter), influenza A virus (IAV – spherical, 80–120 nm in diameter), and tobacco-mosaic virus (TMV – elongated cylinder, 15–18 nm in diameter and around 300 nm in length) in complex buffers. They prepared the sensor surface in multiple steps. They first coated the surface with streptavidin and then with biotinylated antibody layer. While they checked surface roughness, a uniform and temporal constant background was observed. If a smooth and low-rough surface was not obtained at first, they kept saturating the surface with antibodies to obtain a low roughness in order to lower the background and to be able to distinguish the VLPs from background roughness. As seen in Figure 8B, after subtraction of the background, spherical IAV particles (a) and HIV-VLP (b) were characterized. The binding event is also confirmed with the intensity increase and stabilization in the SPR signal in Figure 8B (c) and (d), which is correlated with the size of the particle. However, binding of TMV could not be visualized due to its smaller size in diameter and vanishing on the surface roughness. Even though the surface modification with antibodies was successful and enough for the visualization of ~100-nm-sized viral particles, it was limited for imaging of smaller particles due to the crudity of the sensor surface.

Moreover, in a study where the optimal conditions for SPR imaging of nano-objects are discussed, it has been explained that the layer on the sensor surface and its roughness have great importance in local reflectivity resonance and in signal-to-background ratio [81]. In order to have this high ratio, the reflectivity should be minimum; however, due to the roughness and inhomogeneity of the substrate and the layer on the surface, the achievable minimum reflectivity is limited, which can be obtained as minimum as 1%. The authors were able to lower this by using different techniques to prepare the substrate surface such as magnetron sputtering of gold on glass yielding a proper thickness and 0.1% reflectivity [81].

Limitations emanating from illumination profile necessitate a higher surface sensitivity compared to other types of microscopy such as confocal-based microscopy. Although the use of dark-field microscopy has been moderately explored in detection of BNPs, dielectric nanoparticles and virus particles have been successfully detected using TIR-based dark-field microscopy with sensitivity down to ~100 nm for virus particles [31, 82]. Moreover, in order to improve sensitivity and obtain a more uniform illumination profile, in addition to TIR illumination *via* a prism or an objective, planar waveguides can be used in the evanescent-field microcopy. The sample can be placed in the core layer of the waveguide, which is then exposed to the evanescent part of the guided light in a similar way to TIR illumination [83, 84]. As a result of this configuration, even though the penetration depth of and evanescent field is around 100–200 nm, the depth of evanescent field can be regulated from 100 nm to a micron *via* tuning the thickness and refractive indices of the core and cladding layers of the waveguide [85]. With an evanescent light-scattering microscopy technique, a simultaneous fluorescent and high sensitivity scattering imaging has been done for efficient detection surface binding of BNPs in a label-free way [80]. As well as all the other techniques, in this technique, in order to obtain the highest sensitivity based on evanescent illumination, background scattering must be suppressed. Therefore, a three-layer waveguide design was utilized. For refractive index matching and repressing the roughness of the core layer (root-mean-square surface roughness <1 nm), a silica core layer in between organic fluorinated polymer (CYTOP) cladding layers was used. By this way, the stray lights were reduced while the signal-to-background ratio was improved by enhancing the scattered light coming from the BNPs in aqueous environment. Single lipid vesicles were visualized with scattered and fluorescent light for demonstration as seen in Figure 8C. Individual lipid vesicles (~150-nm diameter) were capture on the sensor surface *via* specific protein receptor binding, and their size was determined. Moreover, after confirmation with a fluorescent dye, the same labeling was also achieved with 18-nm-gold nanoparticles in order to prove the applicability of the technique with very small gold nanoparticle for studying single molecule interaction with surface-immobilized

vesicles. In addition to labeling, molecular interaction on the surface bound vesicles was also determined with the same technique with high sensitivity. To do so, the surface of the silica region of the waveguide was modified with a layer of polymer called PLL-*g*-PEG/PLL-*g*-PEG-biotin for immobilization of lipid vesicles. It is known that this modification provides a low-rough surface and mediates strong binding, while it protects the nature of the molecular interaction and prevents unspecific binding of other biological molecules in the solution [86]. IgG binding to immobilized-lipid vesicles was monitored in scattering mode with a scattering intensity change.

Nearly all of the considerations mentioned earlier, regarding the impact of surface functionalization on the performance on SPR/SPRi biosensors, are applicable to interference reflectance BNP detectors as well. There are, however, a few salient differences. First, while SPR/SPRi biosensors utilize SPP waves that are confined to a narrow region above the gold film interface, interference reflectance sensors detect only far-field scattering. Second, as SPP waves are highly directional, SPP diffraction from a BNP creates a relatively large (with respect to the far-field diffraction limit) and asymmetric feature in the SPRi reflectance image. By comparison, interference reflectance sensors are nearly always diffraction-limited imaging systems that register the presence of a BNP as a symmetric point spread function. Together, these differences may provide reason enough to believe that interference reflectance imaging is more suitable for the detection and characterization of BNPs. Consider that interference reflectance is much less sensitive to variations in the optical thickness of the surface coating, which can be different for two different protein spots, even on the same chip. Additionally, the extended and asymmetric effect of a BNP on the propagating SPPs may reduce the maximum number or density of BNPs that can be captured onto the sensor before they can no longer be enumerated, lowering the dynamic range – although dynamic measurement may be able to ameliorate this problem.

As mentioned earlier, IRIS has been used for VSV detection *via* surface-immobilized antibody probes [87]. In this study, the binding of viral particles to VSV-specific antibody spots was compared with non-specific antibody spots as a negative control, with a limit of detection of 3×10^5 PFU/ml. Very small binding of virions above the background was observed [Figure 9A (a)]. Note that in this study, captured BNPs were not detected individually – instead, an ensemble measurement was made by monitoring the reflectivity spectrum of the surface. In later studies, a high numerical aperture objective was used to detect the faint interference signal from individual virions. Calculating the size of a particle from the brightness of the resulting spot was nontrivial, because increasing the particle size increases the position of its centroid above the reflecting surface, thereby slightly increasing the optical path length difference between forward- and back-scattered light [24]. Once the substrate film thickness and surface morphology were optimized, individual BNPs ranging from 50 nm to 200 nm were detected by affinity-based capture in various complex media with SP-IRIS [88]. Specifically, *vesicular stomatitis* virus (VSV) BNPs with an ellipsoidal shape of around 70×180 nm were captured on antibody-immobilized sensor surfaces and individually counted as seen in Figure 9B. Even though various complex media such as serum or whole blood were used, background noise was reduced by eliminating nonspecific binding of particles with different sizes. In this study as well as others, proper surface morphology and functionalization were achieved *via* coating the sensor surface with a non-fouling copoly-(DMA-NAS-MAPS) polymer [58, 90]. The ssDNA and antibody capture probes were immobilized on the polymer under certain conditions to obtain the perfect spot morphology. The layered surface was checked *via* IRIS, and the thickness of ssDNA and antibody spots was determined after each modification. Thus, the smooth, uniform, and low-rough surface morphology was confirmed before further steps. In order to have a better spot morphology and target capture efficiency, the authors immobilized antibody probes *via* DNA-directed immobilization (DDI). For this, antibodies were conjugated with 40-mer-long oligonucleotides. The complementary sequences of these ssDNAs were selected as the surface probes. ssDNA surface probes were immobilized on the sensor surface. The chips were then incubated with the antibody-DNA conjugates; therefore, anti-VSV antibodies were immobilized on the sensor surface with DNA bridges. This hybridization was also confirmed with IRIS measurements, and surface roughness is validated. Although many layers of modification have been done on the sensor, as the roughness was appropriate and confirmed with low-magnification measurements, captured VSVs were easily distinguished from the background yielding a high signal-to-noise ratio. Moreover, same experiments also were repeated with direct antibody immobilization. When the VSV-capture results were compared, it was shown that DDI improved surface morphology and probe density on the surface; hence, a much higher dynamic range was obtained with DDI-antibody spots. Furthermore, as the recognition sites of the capture antibodies were more available and the antibodies more flexibly tethered, much less total antibodies were needed to achieve the same binding affinity of the spot. Specifically, equivalent virus

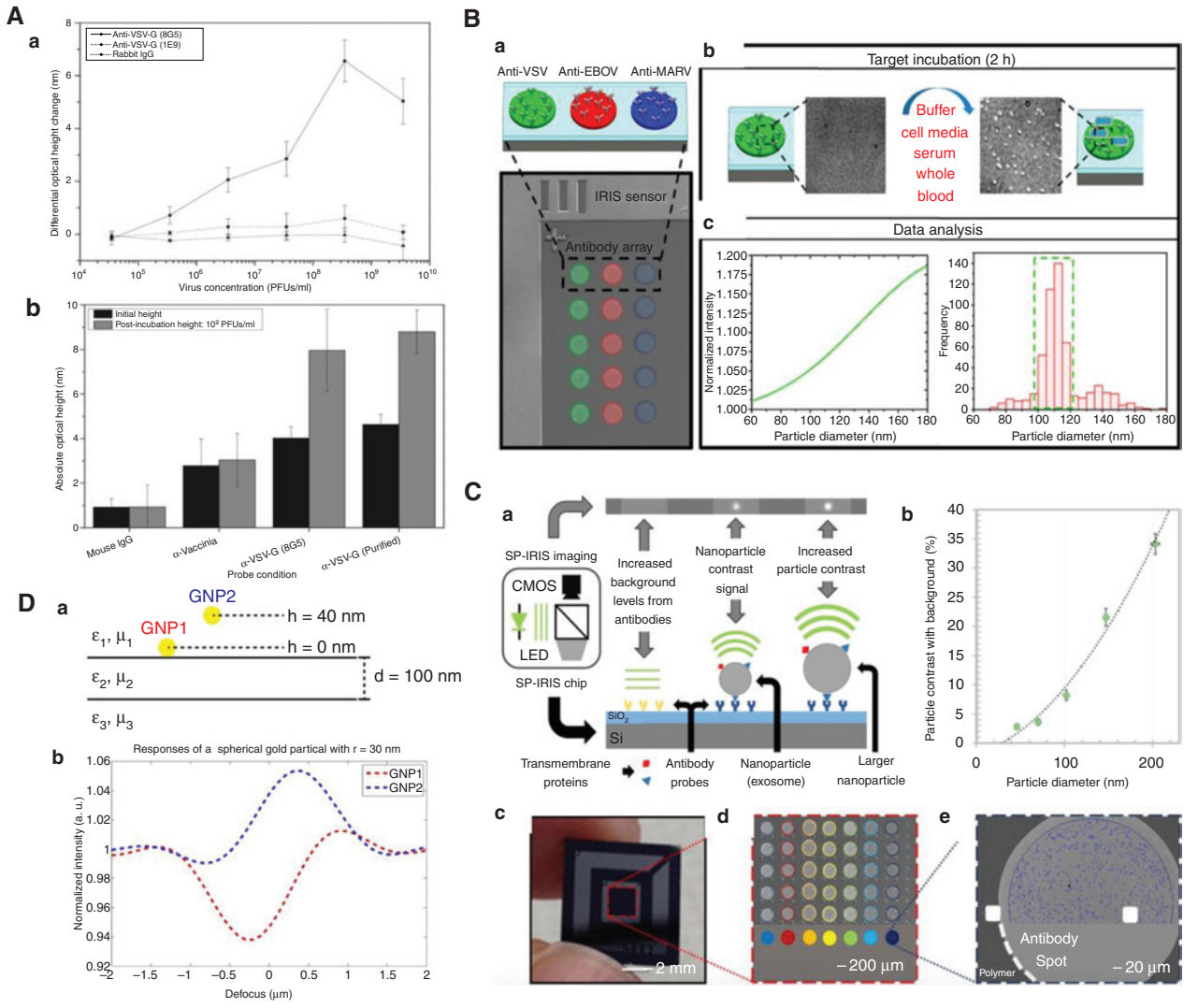

Figure 9: (A) (a) A calibration curve for wild-type VSV (8G5) sample tested with IRIS platform. Corresponding height changes upon specific virion particle binding is shown. Greater binding indicates the greater affinity to immobilized antibody on the sensor. (b) Specific binding and low non-specific binding are shown in the results of pre- and post-incubations with the virions. Adapted from [87]. (B) (a) A SP-IRIS microarray configuration with immobilized antibody spots in green, red, and blue for anti-VSV, anti-EBOV, and anti-MARV probes, respectively. (b) Data acquisition and analysis for virus identification using SP-IRIS. Captured VSV particles can be seen on anti-VSV antibody spotted sensor surface (right) when compared to pre-incubation image (left). (c) The model used for determining the size of each particle within the spot (left) and a size distribution of particles identified on the spot of the image (right). The selected region on the plot represents expected sizes of VSV. Adapted from [88] (Reprinted with permission from [88]. Copyright 2014 American Chemical Society). (C) (a) Schematic representation of the SP-IRIS detection principle (b) SP-IRIS signal for polystyrene nanoparticles with a diameter from 50 to 200 nm used to be reference for exosomes. (c) An image of the SP-IRIS chip. (d) IRIS image of immobilized antibody surface probes. (e) SP-IRIS image of captured particles on the spot, which are detected *via* NVDX analysis. Adapted from [38]. (D) SP-IRIS measurement of spherical gold nanoparticles (r = 30 nm) at (a) h = 0 nm (GNP1) and h = 40 nm (GNP2), and (b) their interferometric responses (GNP1 shown in red, and GNP2 shown in blue). Adapted from [89].

capture was observed even when the average surface density of antibodies was 6× lower. Finally, as the spot printing was performed with only DNA oligonucleotides, the spot uniformity and smoothness as well as process repeatability was greatly improved.

In another study, real-time rapid counting of virus was performed in serum samples using SP-IRIS [39]. The surface of the SP-IRIS chip and setup were modified with antibodies as a highly sensitive rapid detection platform for pathogen detection with minimal sample preparation. Captured VSV particles on the sensor represented higher signals and with the optimal surface chemistry described earlier; no non-specific binding coming from the complex media was observed. As a result, VSV-Ebola model was

detected at a concentration of as low as 100 PFU/ml in less than 30 min.

Moreover, digital exosome detection was demonstrated using SP-IRIS (Figure 9C) [38]. In this study, the size and multi-phenotype information from the same exosome were obtained. The size distribution for the exosomes from HEK 293 cell line was determined as 50–200 nm. Despite being very low refractive index and at very low concentrations in the real samples, with properly immobilized antibodies and smooth background, exosomes were captured and digitally counted with a detection limit of 3.94×10^9 particles/ml, which is very sensitive compared to conventional characterization techniques. Detection and characterization are two different problems for BNPs. Even though the detection is possible with these techniques, characterization needs to be done with the proper instrumentation and surface chemistry. Here, it is important to determine the size of the exosome particles. In order to determine the size, the surface roughness must be small enough to be able to differentiate between the BNPs as specific elevation of NPs due to surface morphology affects the perceived size as seen in Figure 9D [89].

Interferometric scattering microscopy (iSCAT) also depends on the background during the measurements. Although the polarizability of the nano-object is large enough and there is no theoretical limit for detection, the limit stems from the nature of the background where the nano-object of interest presents. iSCAT can reach high signal-to-noise ratio in real-time measurements of localized nanoparticles. In a study, detection and tracking of single, unlabeled 45-nm Simian virus 40 (SV40) virions were shown [91]. The authors obtained an average contrast of $3.00 \pm 0.87\%$ for the scattering signal relative to the background on a glass substrate. Moreover, the binding of virions to receptor proteins in supported membrane bilayers on the sensor surface was tracked with iSCAT. However, as the authors stated, as all the measurements were performed on plasma cleaned-glass substrates, this technique is yet suitable for imaging or tracking nano-objects in strongly scattering media such as serum or intact cell.

4 Conclusion

Biological nanoparticles are significant features in medicine and biomedical research. For the oncologist or immunologist, exosome vesicles contain a wealth of diagnostic information. Similarly, virologists and infectious disease epidemiologists demand and deserve better methods for the rapid and accurate detection and identification of viruses and virus-like particles. An impressive variety of methods have been developed with the goal of addressing this need. Among them, the so-called label-free methods tend to be the most rapid, for example, they been used to measure an effective virus titer, directly from the sample, in mere minutes.

Although the readout technology for these label-free methods is diverse, they all utilize some type of surface coating to provide molecular "recognition" for the targeted BNP. The sensor surface is thereby "functionalized"; without such coatings, label-free methods cannot differentiate between two exosomes, for example, of similar size but different surface antigens. By far, the most common way to functionalize a detector surface is to coat it with a monolayer of "capture" molecules, which have high molecular affinity for a surface antigen on BNP. The diversity of capture molecules – peptides, antibodies/antibody fragments, nucleic acid aptamers, etc. – is accompanied by an even more diverse set of chemical methods of covalently linking them to a variety of surface materials.

Designing an effective surface functionalization has many application-specific requirements. For example, the charge, conformal flexibility, surface density/distribution, and non-fouling properties are often essential performance characteristics for many label-free biosensor surface functionalization. Certain sensing methods described earlier – for example, SPRi – require the surface be a particular material and therefore limit available options.

The quality of the surface coating, therefore, has an enormous impact on the performance (sensitivity, specificity, and speed) of the overall detector. This is even more true in the case of label-free, single-particle biosensors. While label-free biosensors have historically been less sensitive than direct molecular methods (e.g. nucleic acid amplification or enzymatic assays), this has begun to change with the advent of sensors that enumerate the absolute number of BNPs immobilized on the sensor. In the ideal case, these highly sensitive methods are limited only by the shot noise associated with the independent capture of individual particles within a finite sampling window. For instance, if the instrument detects five particles within a particular time interval, it is not unlikely that repeating this measurement a second time with the same interval would yield four or six particles instead. However, there is almost always additional uncertainty as the signal-to-noise ratio of the biosensing instrumentation is not infinite. Here, too, the quality of the surface functionalization does have an impact on the total assay performance. In the case of label-free imaging sensors, the nanoscale

roughness of the sensing surface can be a source of considerable noise. There are several methods that have been used to improve the quality (smoothness) of protein surface coatings, chief among them DNA-directed immobilization of virus-specific antibodies.

Label-free detectors of biological nanoparticles have a wide variety of applications in medicine and biological research. Utilizing appropriate surface functionalization methods can greatly improve the sensitivity, speed, and flexibility of these techniques.

References

[1] Hooke R. Micrographia: or, some physiological descriptions of minute bodies made by magnifying glasses. London, UK, J. Martyn and J. Allestry, 1665.

[2] Fara P. A microscopic reality tale. Nature 2009;459:642–4.

[3] The Nobel Prize in Chemistry 2014. Nobelprize.org. Nobel Media AB 2014. (Accessed November 21, 2016, at http://www.nobelprize.org/nobel_prizes/chemistry/laureates/2014/).

[4] Somers CM, Mc Carry BE, Malek F, Quinn JS. Reduction of particulate air pollution lowers the risk of heritable mutations in mice. Science 2004;304:1008–10.

[5] Yezhelyev MV, Gao X, Xing Y, Al-Hajj A, Nie S, O'Regan RM. Emerging use of nanoparticles in diagnosis and treatment of breast cancer. Lanset Oncol 2006;7:657–67.

[6] Cao Y, Li J, Liu F, et al. Consideration of interaction between nanoparticles and food components for the safety assessment of nanoparticles following oral exposure: a review. Environ Toxicol Pharmacol 2016;46:206–10.

[7] Luo L, Zhang Z, Hou L. Development of a gold nanoparticles based chemiluminescence imaging assay and its application. Anal Chim Acta 2007;584:106–11.

[8] Hendrix RW, Smith MC, Burns RN, Ford ME, Hatfull GF. Evolutionary relationships among diverse bacteriophages and prophages: all the world's a phage. Proc Natl Acad Sci USA 1999;96:2192–7.

[9] Suttle CA. Viruses in the sea. Nature 2005;437:356–61.

[10] DeSantis AMC, Cheng W. Label-free detection and manipulation of single biological nanoparticles. WIREs Nanomed Nanobiotechnol 2016;8:717–29.

[11] Mansuy JM. Mobile laboratories for Ebola and other pathogens. Lancet Infect Dis 2015;15:1135.

[12] Beard JW. Physic chemic characteristics of viruses. Annu Rev Microbiol 1951;5:267–76.

[13] Brooks GF, Carroll KC, Butel JS, Morse SA, Mietzner TA. General properties of viruses. In: Brooks GF, Carroll KC, Butel JS, Morse SA, Mietzner TA, eds. Jawetz, Melnick, & Adelberg's Medical Microbiology, 26e. New York, NY, McGraw-Hill, 2013. (Accessed November 21, 2016 at http://accessmedicine.mhmedical.com/content.aspx?bookid=504&Sectionid=40999951).

[14] Gefroh E, Dehghani H, McClure M, Connell-Crowley L, Vedantham G. Use of MMV as a single worst-case model virus in viral filter validation studies. PDA J Pharm Sci Technol 2014;68:297–311.

[15] Gustafsson S, Mihranyan A. Strategies for tailoring the pore-size distribution of virus retention filter papers. ACS Appl Mater Interfaces 2016;8:13759–67.

[16] Silverton EW, Navia MA, Davies DR. Three-dimensional structure of an intact human immunoglobulin. Proc Natl Acad Sci USA 1977;74:5140–4.

[17] Thery C, Ostrowski M, Segura E. Membrane vesicles as conveyors of immune responses. Nat Rev Immunol 2009;9:581–93.

[18] Zhang J, Li S, Li L, et al. Exosome and exosomal microRNA: trafficking, sorting, and function. Genomics Proteomics Bioinformatics 2015;13:17–24.

[19] Im H, Huilin S, Park YI, et al. Label-free detection and molecular profiling of exosomes with nano-plasmonic sensor. Nat Biotech 2014;32:490–5.

[20] Van der Pol E, Hoekstra AG, SturkA, Otto C, van Leeuwen TG, Nieuwland R. Optical and non-optical methods for detection and characterization of microparticles and exosomes, Thromb Haemostasis 2010;8:2596–607.

[21] Vlassov AV, Magdaleno S, Setterquist R, Conrad R. Exosomes: current knowledge of their composition, biological functions, and diagnostic and therapeutic potential. Biochim Biophys Acta 2012;1820:940–8.

[22] Kulzer F, Orrit M. Single-molecule optics. Annu Rev Phys Chem 2004;55:585–611.

[23] Moerner WE, Fromm DP. Methods of single-molecule fluorescence spectroscopy and microscopy. Rev Sci Instrum 2003;74:3597–619.

[24] Trueb J, Avci O, Sevenler D, Connor JH, Ünlü MS. Robust visualization and discrimination of nanoparticles by interferometric imaging. IEEE J Sel Topics Quantum Electron 2017; 23:1–10.

[25] Patolsky F, Zheng G, Hayden O, Lakadamyali M, Zhuang X, Lieber CM. Electrical detection of single viruses. Proc Natl Acad Sci USA 2004;101:14017–22.

[26] Stern E, Wagner R, Sigworth FJ, Breaker R, Fahmy TM, Reed MA. Importance of the debye screening length on nanowire field effect transistor sensors. Nano Lett 2007;7:3405–9.

[27] Luo X, Xu J, Zhao W, Chen H. Glucose biosensor based on ENFET doped with SiO_2 nanoparticles. Sens Actuators B Chem 2004;97:249–55.

[28] Sant W, Pourciel M, Launay J, Do Conto T, Martinez A, Temple-Boyer P. Development of chemical field effect transistors for the detection of urea. Sens Actuators B Chem 2003;95:309–14.

[29] Sevenler D, Lortlar-Ünlü N, Ünlü S. Nanoparticle biosensing with interferometric reflectance imaging. In: Vestergaard MC, Kerman K, Hsing IM, Tamiya E, eds. Nanobiosensors and Nanobioanalyses. Springer, Japan, 2015:81–95.

[30] Faez S, Lahini Y, Weidlich S, et al. Fast, label-free tracking of single viruses and weakly scattering nanoparticles in a nanofluidic optical fiber. ACS Nano 2015;9:12349–57.

[31] Enoki S, Iino R, Morone N, et al. Label-free single-particle imaging of the influenza virus by objective-type total internal reflection dark-field microscopy. PLoS One 2012;7:e49208.

[32] Scarano S, Scuffi C, Mascini M, Minunni M. Surface plasmon resonance imaging (spri)-based sensing: a new approach in signal sampling and management. Biosens Bioelectron 2010;26:1380–85.

[33] Ortega-Arroyo J, Kukura P. Interferometric scattering microscopy (iSCAT): new frontiers in ultrafast and ultrasensitive optical microscopy. Phys Chem Chem Phys 2012;14:15625–36.

[34] Özkumur E, Yalçın A, Cretich M, et al. quantification of DNA and protein adsorption by optical phase shift. Biosens Bioelectron 2009;25:167–72.
[35] Shpacovitch V, Temchura V, Matrosovich M, et al. Application of surface plasmon resonance imaging technique for the detection of single spherical biological submicrometer particles. Anal Biochem 2015;486:62–9.
[36] Sevenler D, Ünlü MS. Numerical techniques for high-throughput reflectance interference biosensing. J Mod Opt 2016;62:1115–20.
[37] De Wit G, Danial JSH, Kukura P, Wallace MI. Dynamic label-free imaging of lipid nanodomains. Proc Natl Acad Sci USA 2015;112:12299–303.
[38] Daaboul GG, Gagni P, Benussi L, et al. Digital detection of exosomes by interferometric imaging. Sci Rep 2016;6:37246.
[39] Scherr SM, Daaboul GG, Trueb J, et al. Real-time capture and visualization of individual viruses in complex media. ACS Nano 2016;10:2827–33.
[40] Scherr SM, Freedman DS, Agans KN, et al. Disposable cartridge platform for rapid detection of viral hemorrhagic fever viruses. Lab Chip 2017;17:917–25.
[41] Vahala KJ. Optical microcavities. Nature 2003;424:839–46.
[42] Su J, Goldberg AFG, Stoltz BM. Label-free detection of single nanoparticles and biological molecules using microtoroid optical resonators. Light Sci Appl 2016;5:e16001.
[43] Armani AM, Kulkami RP, Fraser SE, Flagan RC, Vahala KJ. Label-free single-molecule detection with optical microcavities. Science 2007;317:783–7.
[44] Hu RM, Novo C, Funston A, et al. Dark-field microscopy studies of single metal nanoparticles: understanding the factors that influence the linewidth of the localized surface plasmon resonance. J Mater Chem 2008;18:1949–60.
[45] Hecht E. Optics (4th edition) Reading, MA, USA, Addison-Wesley, 2002.
[46] Méjard R, Griesser HJ, Thierry B. Optical biosensing for label-free cellular studies. Trends Analyt Chem 2014;53:178–86.
[47] Kihm KD. Surface plasmon resonance reflectance imaging technique for near-field (~100 nm) fluidic characterization. Exp Fluids 2010;48:547–64.
[48] Wang S, Shan X, Patel U, et al. Label-free imaging, detection, and mass measurement of single viruses by surface plasmon resonance. Proc Natl Acad Sci USA 2010;107:16028–32.
[49] Verschueren H. Interference reflection microscopy in cell biology: methodology and applications. J Cell Sci 1985; 75:279–301.
[50] Davidson M, Kaufman K, Mazor I, Cohen F. An application of interference microscopy to integrated circuit inspection and metrology. Proc SPIE 1987;775:233–49.
[51] Montgomery PC, Benatmane A, Fogarassy E, Ponpon JP. Large area, high resolution analysis of surface roughness of semiconductors using interference microscopy. Mat Sci Eng B-Solid 2002;91:79–82.
[52] Rothmund M, Schütz A, Brecht A, Gauglitz G, Berthel G, Gräfe D. label free binding assay with spectroscopic detection for pharmaceutical screening. Fresenius J Anal Chem 1997;1:15–22.
[53] Piliarik M, Sandoghdar V. Direct optical sensing of single unlabelled proteins and super-resolution imaging of their binding sites. Nat Commun 2014;5:4495.
[54] Daaboul GG, Vedula RS, Ahn S, et al. LED-based interferometric reflectance imaging sensor for quantitative dynamic monitoring of biomolecular interactions. Biosens Bioelectron 2011;26:2221–7.
[55] Melanie E, Le Blanc AF, Gauglitz G, Proll G. A robust sensor platform for label-free detection of anti-salmonella antibodies using undiluted animal sera. Anal Bioanal Chem 2013;405:6461–9.
[56] Daaboul GG, Yurt A, Zhang X, Hwang GM, Goldberg BB, Ünlü MS. High-throughput detection and sizing of individual low-index nanoparticles and viruses for pathogen identification. Nano Lett 2010;10:4727–31.
[57] Kukura P, Ewers H, Müller C, Renn A, Helenius A, Sandoghdar V. High-speed nanoscopic tracking of the position and orientation of a single virus. Nat Methods 2009;6:923–7.
[58] Seymour E, Daaboul GG, Zhang X, et al. DNA-directed antibody immobilization for enhanced detection of single viral pathogens. Anal Chem 2015;87:10505–12.
[59] Beuthand J, Minet O, Helfmann J, Herrig M, Müller G. The spatial variation of the refractive index in biological cells. Phys Med Biol 1996;41:369–82.
[60] Svet VD. About holographic (interferometric) approach to the primary visual perception. Open Open J Biophys 2013;3:165–77.
[61] Melnik EVA, Bruck R, Hainberger R, Lämmerhofer M. Multi-step surface functionalization of polyimide based evanescent wave photonic biosensors and application for DNA hybridization by Mach-Zehnder interferometer. Anal Chim Acta 2011;699:206–15.
[62] Fan X, White IM, Shopova SI, Zhu H, Suter JD, Sun Y. Sensitive optical biosensors for unlabeled targets: a review. Anal Chim Acta 2008;620:8–26.
[63] Kausaite-Minkstimiene A, Ramanaviciene A, Kirlyte J, Ramanavicius A. Comparative study of random and oriented antibody immobilization techniques on the binding capacity of immunosensor. Anal Chem 2010;82:6401–8.
[64] Doern GV, Herrmann JE, Henderson P, Stobbs-Walro D, Perron DM, Blacklow NR. Detection of rotavirus with a new poly- clonal antibody enzyme immunoassay (Rotazyme II) and a commercial latex agglutination test (Rotalex): comparison with a monoclonal anti- body enzyme immunoassay. J Clin Microbiol 1986;23:226–9.
[65] Stevens J, Blixt O, Glaser L, et al. Glycan microarray analysis of the hemagglutinins from modern and pandemic influenza viruses reveals different receptor specificities. J Mol Biol 2006;355:1143–55.
[66] Yoo SM, Lee SY. Optical biosensors for the detection of pathogenic microorganisms. Trends Biotechnol 2016;34:7–25.
[67] Levicky R, Horgan A. Physicochemical perspectives on DNA microarray and biosensor technologies. Trends Biotechnol 2005;23:143–9.
[68] Ge D, Wang X, Williams K, Levicky R. Thermostable DNA immobilization and temperature effects on surface hybridization. Langmuir 2012;28:8446–55.
[69] Vollmer F, Arnold S. Whispering-gallery-mode biosensing: label- free detection down to single molecules. Nat Methods 2008;5:591–6.
[70] Hunt HK, Armani AM. Bioconjugation strategies for label-free optical microcavity sensors. IEEE J Sel Top Quant 2014;20:6900213.

[71] Daaboul GG, Lopez CA, Yurt A, Goldberg BB, Connor JH, Ünlü MS. Label-free optical biosensors for virus detection and characterization, IEEE J Sel Top Quant 2012;18:1422–33.
[72] Estevez MC, Otte MA, Sepulveda B, Lechuga LM. Trends and challenges of refractometric nanoplasmonic biosensors: a review. Anal Chim Acta 2014;806:55–73.
[73] Piliarik M, Homola J. Surface plasmon resonance (SPR) sensors: approaching their limits? Opt Express 2009;17:16505–17.
[74] Eddings MA, Eckman JW, Arana CA, et al. "Spot and hop": internal referencing for surface plasmon resonance imaging using a three-dimensional microfluidic flow cell array. Anal Biochem 2009;385:309–13.
[75] Liu J, Eddings MA, Miles AR, Bukasov R, Gale BK, Shumaker-Parry JS. In situ microarray fabrication and analysis using a microfluidic flow cell array integrated with surface plasmon resonance microscopy. Anal Chem 2008;81:4296–301.
[76] Ouellet E, Lausted C, Lin T, Yang CWT, Hood L, Lagally ET. Parallel microfluidic surface plasmon resonance imaging arrays. Lab Chip 2010;10:581–8.
[77] Malic L, Cui B, Veres T, Tabrizian M. Enhanced surface plasmon resonance imaging detection of DNA hybridization on periodic gold nanoposts. Opt Lett 2007;32:3092–4.
[78] Rothenhausler B, Knoll W. Surface–plasmon microscopy. Nature 1988;332:615–7.
[79] Quinn JG, O'Neill S, Doyle A, et al. Development and application of surface plasmon resonance-based biosensors for the detection of cell-ligand interactions. Anal Biochem 2000;281:135–43.
[80] Agnarsson B, Lundgren A, Gunnarsson A, et al. Evanescent light-scattering microscopy for label-free interfacial imaging: from single sub-100 nm vesicles to live cells. ACS Nano 2015;9:11849–62.
[81] Zybin A, Shpacovitch V, Skolnik J, Hergenröder R. Optimal conditions for SPR-imaging of nano-objects. Sens Actuators B Chem 2017;239:338–42.
[82] Ueno H, Nishikawa S, Iino R, et al. Simple dark-field microscopy with nanometer spatial precision and microsecond temporal resolution. Biophys J 2010;98:2014–23.
[83] Thoma F, Langein U, Mittler-Neher S. Waveguide scattering microscopy. Opt Commun 1997;134:16–20.
[84] Ramachandran S, Cohen DA, Quist AP, Lal R. High performance, LED powered, waveguide based total internal reflection microscopy. Sci Rep 2013;3:2133.
[85] Agnarsson B, Ingthorsson S, Gudjonsson T, Leosson K. Evanescent-wave fluorescence microscopy using symmetric planar waveguides. Opt Express 2009;17:5075–82.
[86] Feuz L, Jonsson P, Jonsson MP, Hook F. Improving the limit of detection of nanoscale sensors by directed binding to high-sensitivity areas. ACS Nano 2010;4:2167–77.
[87] Lopez CA, Daaboul GG, Vedula R, et al. Label-free, multiplexed virus detection using spectral reflectance imaging. Biosens Bioelectron 2011;26:3432–7.
[88] Daaboul GG, Lopez CA, Chinnala J, Goldberg BB, Connor JH, Ünlü MS. Digital sensing and sizing of vesicular stomatitis virus pseudotypes in complex media: a model for ebola and marburg detection. ACS Nano 2014;8:6047–55.
[89] Avci O, Adato R, Ozkumur AY, Ünlü MS. Physical modeling of interference enhanced imaging and characterization of single nanoparticles. Opt Express 2016;24:6094–114.
[90] Cretich M, Pirri G, Damin F, Solinas I, Chiari M. A new polymeric coating for protein microarrays. Anal Biochem 2004;332:67–74.
[91] Ewers H, Jacobsen V, Klotzsch E, Smith AE, Helenius A, Sandoghdar V. Label-free optical detection and tracking of single virions bound to their receptors in supported membrane bilayers. Nano Lett 2007;7:2263–6.